CHAPTER 3

RESEARCH METHODS

This chapter outlines the field and laboratory techniques used in this study. It focuses on survey methods, excavations, section scraping and step-trenching strategies, sample preparation and technical procedures used in this thesis rather than providing a detailed treatment of the principles behind each technique as they are long-established methods. Sites which are investigated in detail are summarised in subsection 3.1.2. Further details of each site are discussed in the relevant chapters.

3.1 Field Methods

3.1.1 Explorations

The area under investigation falls between the geo-coordinates of 15º to 16º north latitudes and 79º to 80º east longitudes. This area (~ 10,000 km^2) is drained by three independent east-flowing rivers: the Gundlakamma, the Paleru, and the Manneru. Previous archaeological studies in this region (e.g., Issac, 1960; Kumari, 1987; Rao, 1979; Srinivasulu, 2012) have identified rich Palaeolithic records ranging from Acheulian to Late Palaeoliths. In addition to the rich Palaeolithic record, this region is geologically significant as it has yielded YTT deposits (Reddy & Shah, 2004) and inland sand dunes (Reddy et al., 2013).

The current surveys have identified 68 Primary Palaeolithic sites and seven sites directly associated with YTT deposits. For systematic survey purposes, the whole area (1º X 1º) is divided into 15' X 15' squares; further, each of these 15' X 15' squares is divided into 3' X 3' (~ 6 km X 6 km) squares, which forms the basic unit for exploration (Map. 3.1.1). For each of these 3' X 3' squares, geomorphological, erosional, land use & land cover and DEM maps were made using Bhuvan (Indian Geo-Platform for ISRO) thematic data and satellite images obtained from USGS earth explorer. These maps were analyzed, and potential areas were identified based on their geomorphic association, such as water bodies (including present-day water bodies and topographically low-lying areas/shallow depressions), barren lands, and erosional terrains for explorations. This methodology was applied to explore the three 15 º X 15 º min squares, which yielded 68 Palaeolithic and YTT sites. The artefacts from these sites are in the primary context getting exposed due to erosion in recent times (find spots of artefacts and artefacts within the river channel and secondary context sites are not included in this list of 68).

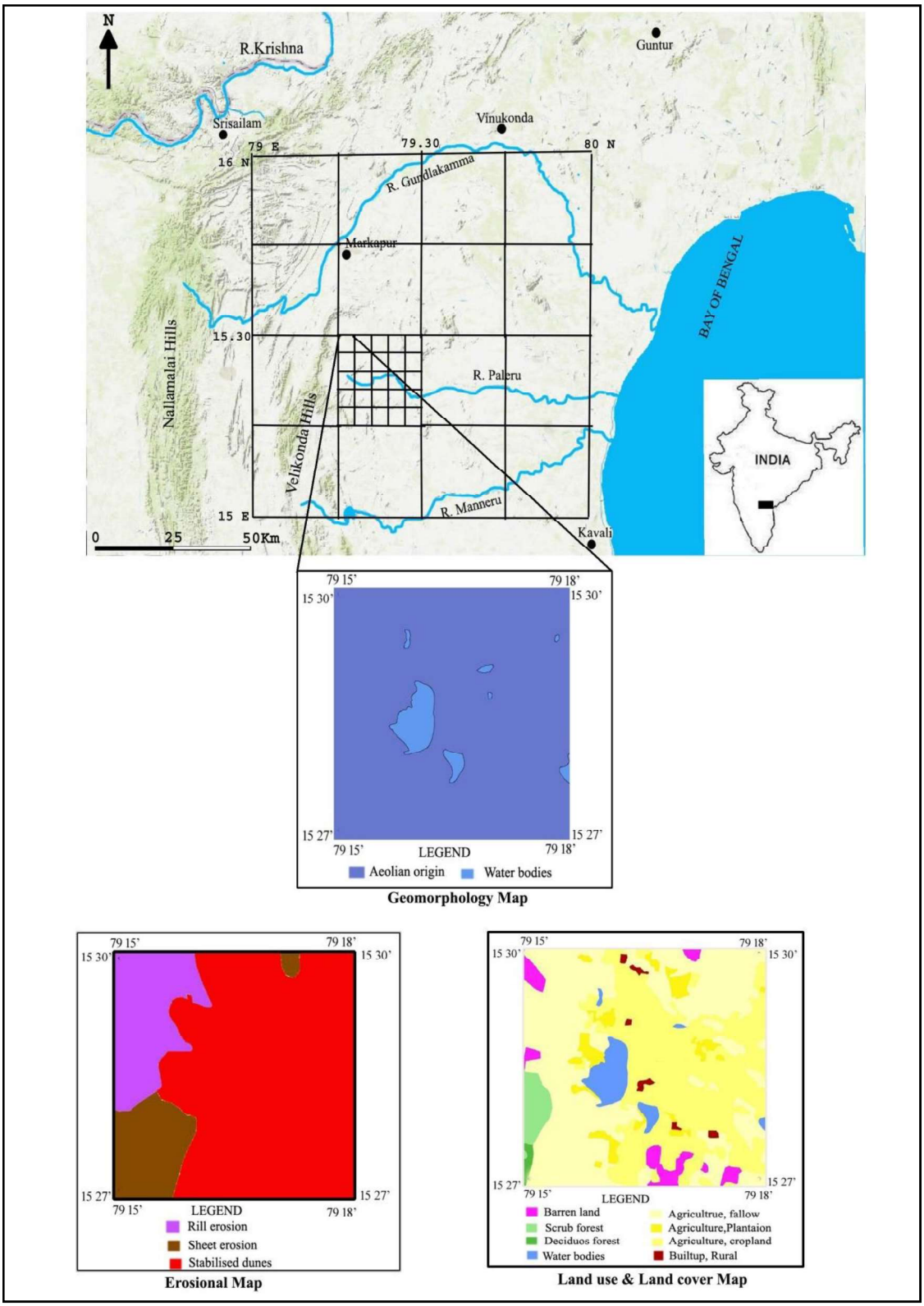

Map. 3.1.1: Thematic representation of the exploration methods.

3.1.2 Excavations, Section Scrapings and Step Trenching

At seven of the newly reported sites, namely A. Agraharam, Nandanavanam, Hanumanthunipadu, Retlapalle, Vemulapadu, Motravulapadu, Ardhaveedu excavations, section scrapings and step trenching were conducted (Table 3.1.1). These sites were chosen for detailed analysis based on the presence of rich lithic material within stratified contexts. Further preliminary analysis of these sites' lithic material indicates that they range temporally from Acheulian to Late Palaeolithic.

Table. 3.1.1: Excavation methods followed for the sites investigated in detail.

Site Name	Method
A. Agraharam	Section Scraping
Nandanavanam	Section Scraping
Hanumanthunipadu	Section Scraping
Retlapalle	Step trench
Vemulapadu	Section Scraping
Motravulapadu	Excavations
Ardhaveedu	Section Scraping

Excavations were done employing a single context recording system, with discrete sediment units separated into 10 cm spits as required. Sediments were screened using a 2 mm sieve to recover micro artefacts. Excavated sections and artefact-bearing horizons were photographed for photogrammetric reconstruction. Sediment was sampled at a 10 cm interval from the entire sections for various geo-archaeological analyses. OSL samples were collected from all sediment units, with the recovery of sediment samples supported by *in situ* background radiation measurements.

In order to increase the artefact sample size, systematic surface materials were also collected at the aforementioned sites (A detailed description of the same is provided in Chapter 4). Several clusters were identified at the sites, grids of different sizes were laid out at rich clusters, and artefacts were collected.

3.2 Laboratory Methods

3.2.1 Geochemical analyses

Toba Ash samples were collected from three sites, Timmayyapalem, Ainavolu, Jadadevi and Retlapalle and analyzed at the Research Laboratory for Archaeology and the History of Art, University of Oxford. Glass and biotite crystals from the tephra layers were characterized using the same methods as those used in Smith et al., (2011) and Blinkhorn et al., (2014).

3.2.2 Particle Size analyses

Particle analyses were conducted for the sediments collected from the Retlapalle step trench. Preparation of the samples for particle size analysis involved first dispersing them in weak hydrochloric acid (0.5 M) to remove carbonates, and they were subsequently treated with 30% Hydrogen peroxide to remove organic matter and then with sodium hexametaphosphate solution (6.2 g of $(NaPO_3)_6$ to 1 L of distilled water) to separate fine particles. The samples were then dried in an oven at 50°C for 36 hours. A Mastersizer 2000 laser granulometer (Malvern Instruments) was used to measure the grain sizes. Dry samples were dispersed in distilled water in the dispersion unit and passed through a cell with a glass window where a laser beam measured the grain sizes. A computer linked to the Mastersizer 2000 collected the data, with data collection repeated five times per sample to check for anomalies in the measurements.

3.2.3 Mineral Magnetics

The mineral magnetic analyses were conducted in the Magnetic Laboratory, Department of Geology, Savitribai Phule University, Pune, India. The samples were homogenized using agate mortar and pestle. The sample was compactly placed into pre-weighted eight cubic centimetres cylindrical non-magnetic plastic containers. The weight of the samples was used to estimate the magnetic parameters on a mass-specific basis.

Magnetic Susceptibility was measured using Bartington Magnetic Susceptibility Meter with Dual Frequency Sensor. The sensor was calibrated using the standard given by the manufacturer. The measurements were carried out in the 0.1 range with the SI unit of $10^{-8}m^3Kg^{-1}$. Magnetic Susceptibility was measured at a low frequency of 0.4 kHz (Xlf) and a high frequency at 4 kHz (Xhf). The frequency-dependent Susceptibility (Xfd) was calculated from Xlf and Xhf values. Anhysteretic Remanent Magnetisation (ARM) was grown in the samples

in a frequency alternating field of 100 mT, whereas the samples were subjected to a steady field of 0.05 mT. The calibration sample provided by the manufacturer was used to calibrate the magnetometer. An AF demagnetizer and an ARM attachment (both of Molspin make) were used. The ARM has grown after demagnetizing was measured using a Molspin spinner magnetometer. The Susceptibility of ARM was converted into a mass-specific ARM (XARM) by dividing it by mass. Natural Remanent Magnetization (NRM) was measured using the Molspin impulse magnetizer by calibrating with the sample provided by the manufacturer. Isothermal Remanent Magnetization (IRM) was grown in steps at different field strengths (25, 50, 100, 200, 300, 400, 500, 700, 800, and 1000 for forward and -10, -20, -30, -40, -50, -70, -100, -300 for backfield) using a Molspin impulse magnetizer. The isothermal remanence grew in a 1 T field representing Saturation Isothermal remanent magnetization (SIRM). All remanence measurements were made using the Molspin Impulse magnetizer. Parametric ratios like SOFTIRM, HARDIRM**,** B(0)CR**,** S-RATIO-100, S-RATIO300, SIRM/XLF, XARM/XLF, NRM/XLF, XARM/Xfd% were estimated to define the mineralogy and grain size of the magnetic minerals.

3.2.4 Optically Stimulated Luminescence dating

Optically Stimulated Luminescence (OSL) dating of the sediments was conducted in the OSL laboratory, AMOPH at Physical Research Laboratory (PRL), Ahmedabad, India. Twenty-one samples from seven sites were measured for the luminescence ages estimations. Samples were collected in sealed metal tubes after cleaning the section by a few cm (>20 cm). Samples were opened and processed under subdued red light. The sample's outer ~3 cm portion was used for moisture content and radioactivity measurements. The interior part of the sample was treated with 1N Hydrochloric (HCl) acid for 24 hours to remove carbonates and with 40% Hydrogen Peroxide (H_2O_2) for 12 hours to remove organic materials (Wintle, 1997). Grains measuring 90-150 μm in diameter were separated through dry sieving. Further, the quartz and feldspar grains were separated using a Frantz® magnetic separator. Selected feldspar grains were subsequently etched with 10% Hydrofluoric (HF) acid for 10 minutes to remove the alpha-irradiated skin (Duval et al., 2018; Goedicke, 1984; Porat et al., 2015). After HF etching, feldspar grains were treated with concentrated HCl (37%) for 30 minutes to dissolve the residual fluorides. Measurements were carried out on single-grain discs in single aliquot mode. The feldspar grains were mounted on these discs containing 100 holes. Grains were stimulated using Infrared (IR) LEDs in a Risø TL/OSL DA-20 reader (Bøtter-Jensen et al., 2003). The

wavelength of IR LEDs peaks at 850 ± 30 nm. The detection of emitted luminescence was done in the blue window using BG-39 and BG-3 filter combination.

Quartz grains from all the samples saturated around 60-70 Gy (Fig. 3.2.1); therefore, the post-IR-IRSL Single Aliquot regeneration (p-IR-IRSL SAR) protocol was used for the estimation of paleo-dose (D_e) (Akhilesh et al., 2018; Buylaert et al., 2009) (Table 3.2.1). We limited the measurements to a maximum of 10 to 12 aliquots for the older samples. We used CAM (central age model) model for all the samples, as the overdispersion was within the accepted range. A preheat of 320º C for 60 s was used, and p-IR-IRSL was measured at 290º C for 100 s (Buylaert et al., 2011); (Thomsen et al., 2011); (Thiel et al., 2011). The preheat temperature was decided based on preheat plateau test. Preheat test was conducted on the natural sample, and an arithmetic mean of equivalent dose (D_e) of 3 aliquots for each preheat was used to draw preheat plateau curve. The initial 1 s luminescence signal was used as the background, and a signal averaged over the last 20 s was used as the background. The doses for 260º C, 280º C, 300º C, and 320º C fell within 5% of the estimated palaeo-dose (Fig 3.2.2).

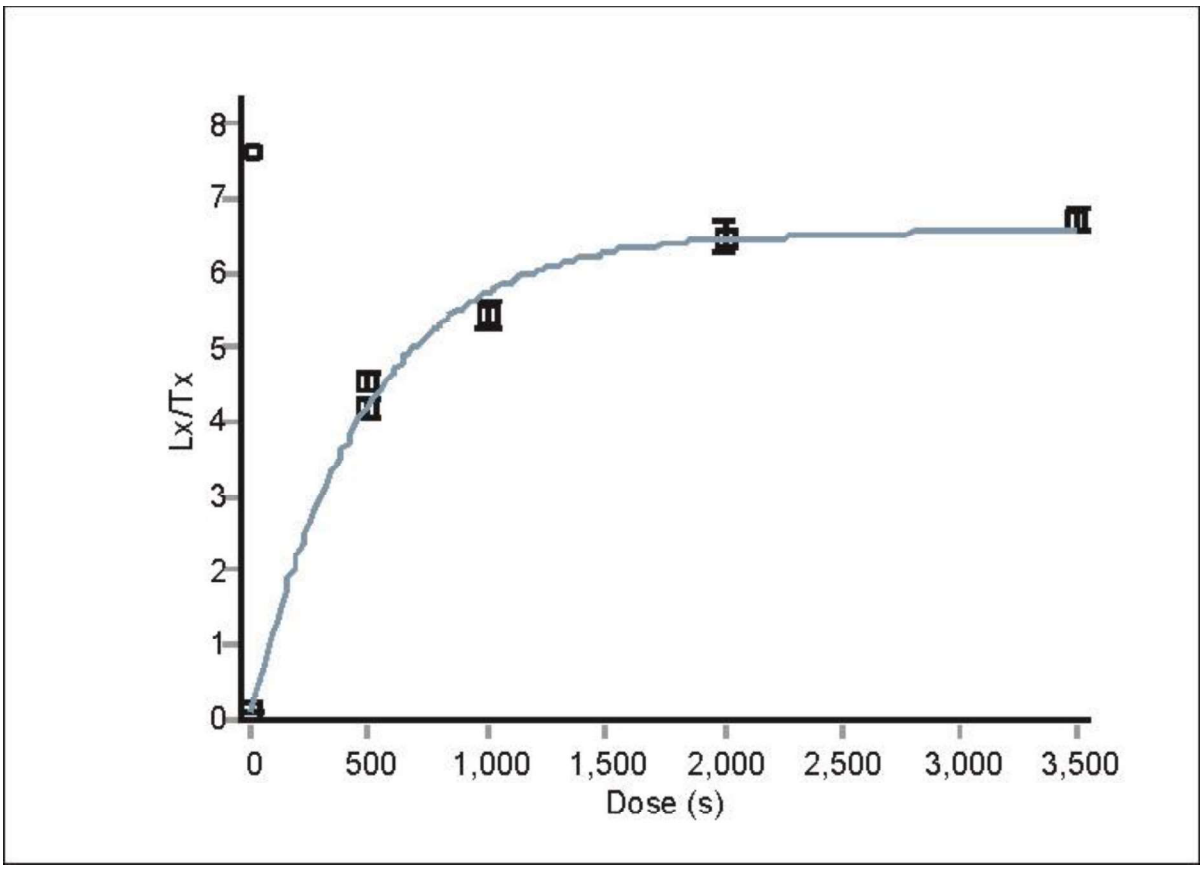

Figure. 3.2.1: Luminescence signal in saturation for the OSL sample from Retlapalle.

A dose recovery test was conducted to test the p-IR-IRSL SAR protocol's applicability. For the dose recovery test, six aliquots were used, and these aliquots were first bleached in the reader using the bleaching step as mentioned in (Table. 3.2.1). To check the residual dose in nature, six aliquots were exposed to 300W Ultra vitalux solar lamp filtered through glass up to 5 hours. The results of the dose recovery test and the residual dose estimation are discussed in Chapter 4 for each site. For all the samples, the acceptance criteria followed were recuperation ratio: 5%, recycling ratio: 10%, and test dose error: 10%. The fading rates (*g*-values) were estimated using the procedure outlined by (Auclair et al., 2003). It involves bleaching the sample and incorporating a known laboratory dose approximately similar to paleo-doses estimated for respective samples, preheating the sample and then measuring luminescence intensity for different time delays. The time delays ranged from prompt measurements to up to 3 days. Fading rate (% per decade) was estimated from the slope of the graph plotted between delayed intensities and logarithmic delayed time.

Table. 3.2.1: Parameters of the p-IR-IRSL SAR protocol.

Step	Treatment	Observed measurement
1	Natural signal	
2	Preheat for 60 s at 320 °C	Remove thermally unstable signal
3	IR stimulation, 100 s at 50 °C	
4	IR stimulation, 100 s at 290 °C	L_x (measured luminescence)
5	Test dose	
6	Preheat, 60 s at 320 °C	Remove thermally unstable signal
7	IR stimulation, 100 s at 50 °C	
8	IR stimulation, 100 s at 290 °C	T_x (measured test dose luminescence)
9	IR stimulation, 200 s at 325 °C	Bleach
10	Give dose and return to step 2	

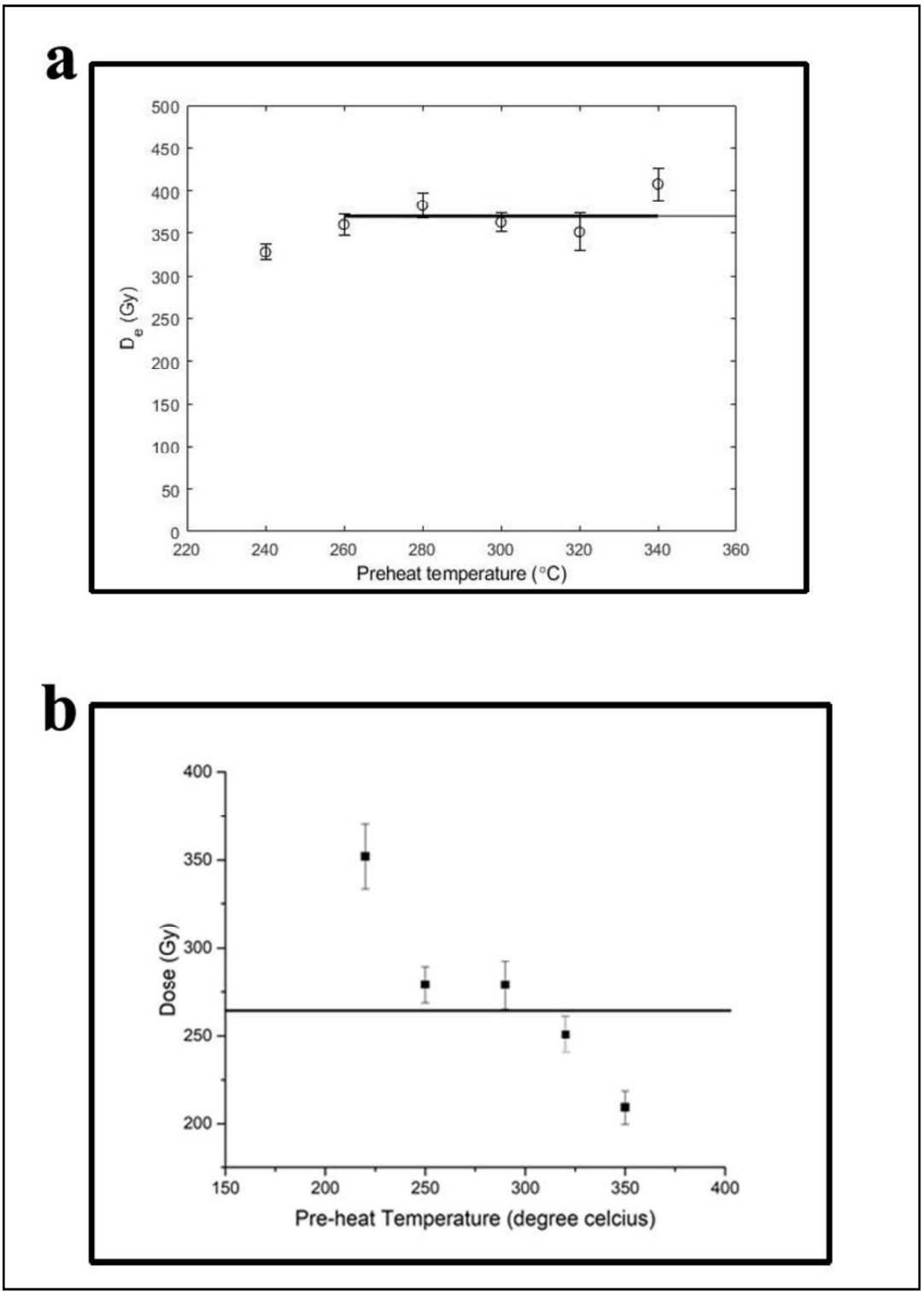

Figure. 3.2.2: Preheat plateau test: equivalent dose (d_e) variation with preheat temperature for the natural samples. At each point, d_e is the arithmetic mean of three values. The error bar is the standard error of the three values. The doses for 260º c, 280º c, 300º c, and 320º c fell within 5% of the estimated paleo-dose. a: Sample from Hanumanthunipadu; b: Sample from Retlapalle.

3.3 Lithic Analyses

Lithic artefacts collected from trenches, section scrapings and systematic surface surveys were washed and labelled. Quantitative and qualitative attributes were recorded for each artefact in the assemblage, except for broken flakes, flaked pieces, and core fragments. Artefacts were categorized into standard technological groups and more formal typological classes wherever suitable (e.g., Core, Flake, Retouched flake, Hand axe, Cleaver, Blade). For typological and technological descriptions of the artefacts, standard terminologies were employed used across South Asia and beyond (e.g., (Akhilesh et al., 2018; Blinkhorn, 2012; Jones, 2007; Zaidner et al., 2018). The same thing applies to the terms used in the formal descriptions of key technologies such as Levallois (Boëda, 1995; van Peer, 1992). For each artefact, a number of metric and non-metric attributes were recorded. For the flake-based (Middle Palaeolithic) and Blade-based assemblages, all attributes were measured following the methods devised by Clarkson & S. O'Conner, (2004); Jones, (2007). For Acheulian assemblages, attributes including length, width, thickness, elongation (length - width ratio), refinement (thickness - width ratio), and plan & profile symmetry were recorded. Symmetry was calculated using the Flip Test (Hardaker & Dunn, 2005; Shipton, 2016; Shipton et al., 2019) for all the bifaces in two planes. Artefacts were photographed and imported into the Flip Test program, and the asymmetry index was calculated without the rotation option. Representative artefacts were photographed for illustration purposes. Metrical details are documented using digital callipers, a weighing scale (WeiHeng®) with a resolution of 0.5 g for accurately weighing artefacts up to 1000 g, a basic mechanical scale for measuring artefacts over 200 g, a protractor with a rotating arm for measuring angles, and a magnifying lens. The list of attributes recorded for the different technological type classes are discussed below with relevant illustrations adopted from Jones, (2007).

The methodology followed in the analysis of lithic artefacts is illustrated in the following diagrams. The technological & typological categories and definitions were adopted from Clarkson & S. O'Conner, (2004); Jones, (2007). The assemblage was divided into broader technological groups such as Biface (including Hand axes and Cleavers), Cores, Unretouched Flakes, Retouched Flakes and Debitage (less than 2 cm in length) (Fig. 3.3.1).

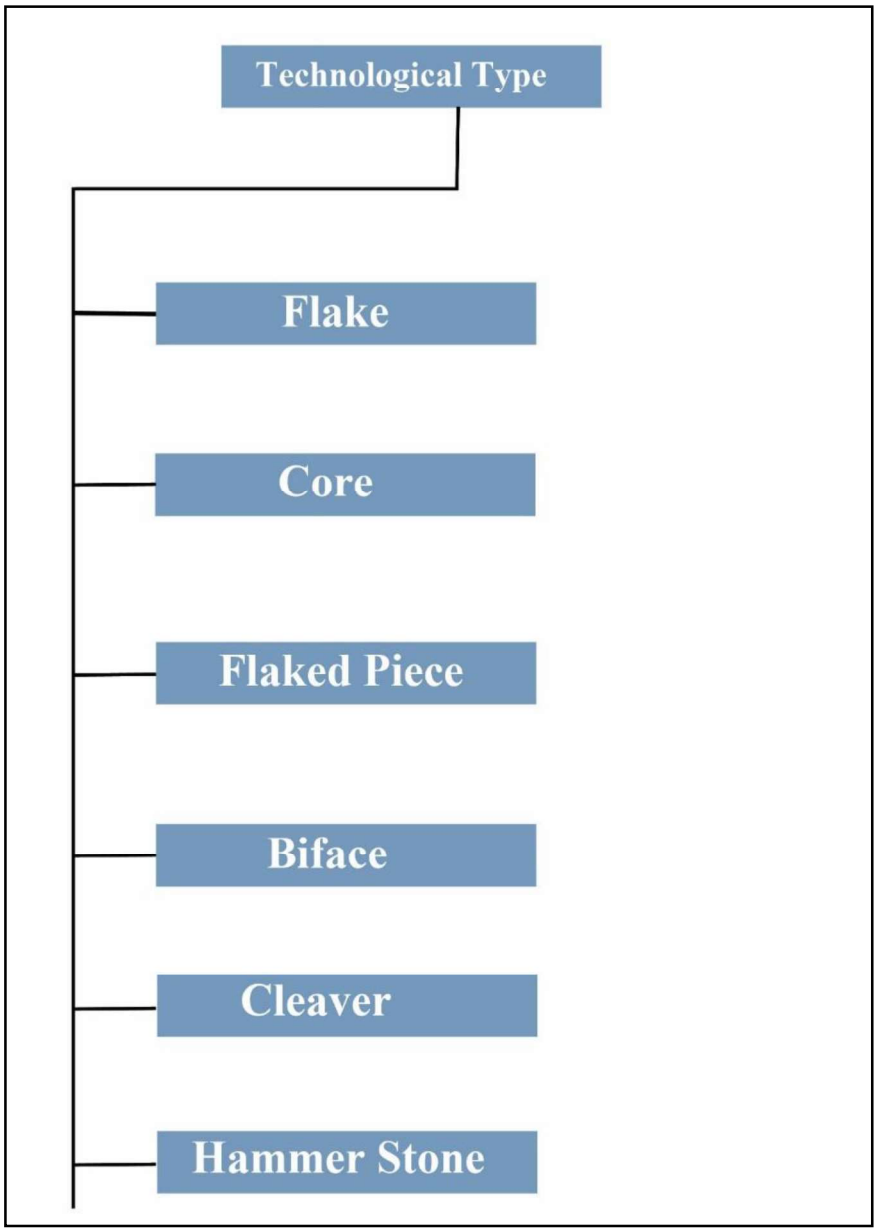

Figure. 3.3.1: Flow chart showing the broader lithic technological classification adopted in this study.

Flakes were further classified by assigning their position in either biface reduction or core reduction sequence based on the characteristics suggested by (Akhilesh & Pappu, 2015; Delagnes, 1993; Newcomer, 1971) (Fig. 3.3.2). Cores were further classified as two broad categories as informal and formal reduction cores (Fig. 3.3.3). Bifacially worked artefacts were classified as Hand axes, cleavers and bifacial points.

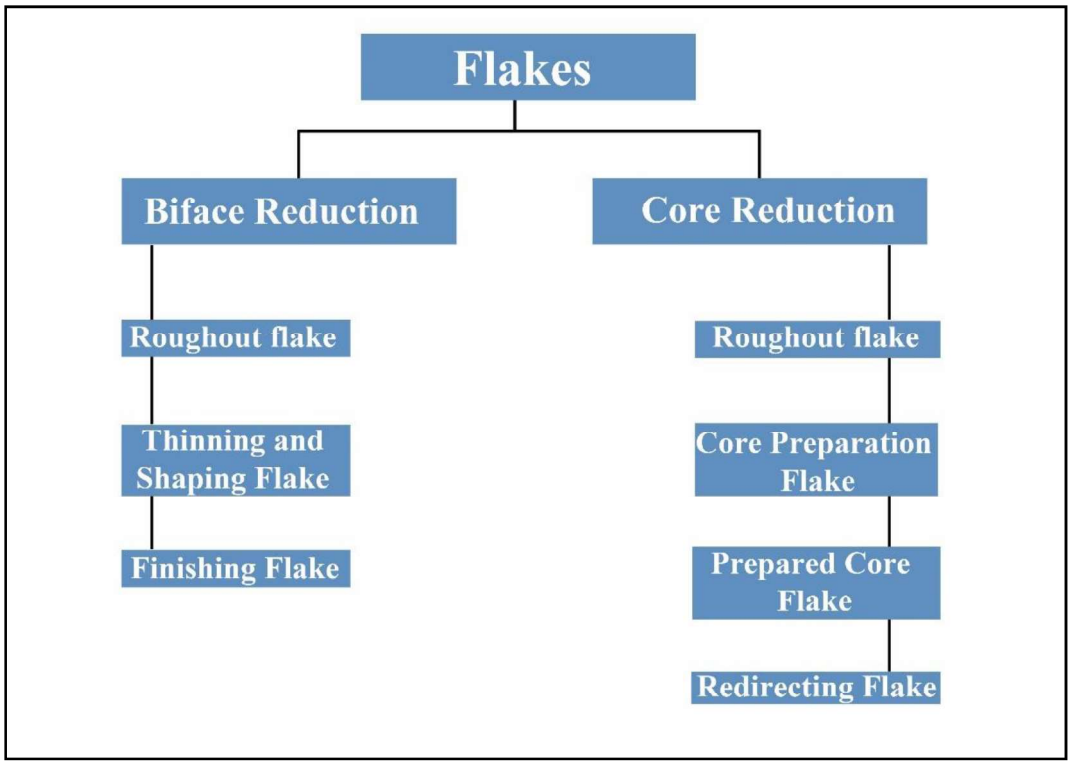

Figure. 3.3.2: Technological Classification of flakes.

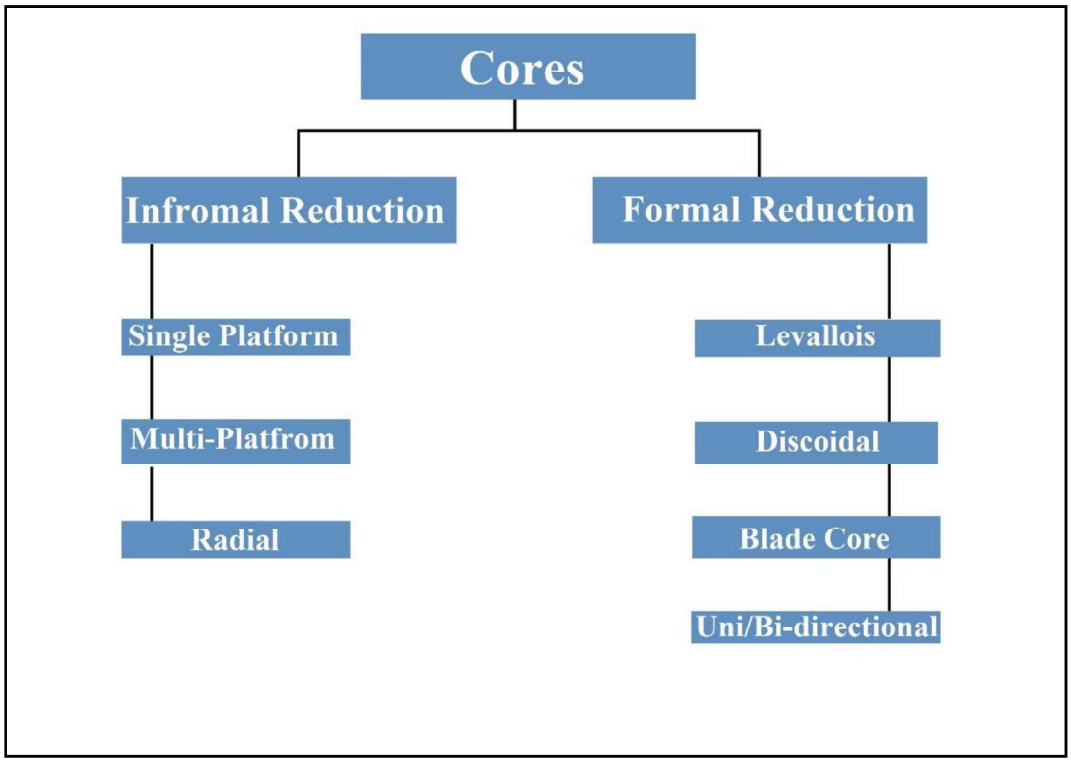

Figure. 3.3.3: Classification of Cores.

Several attributes of flakes, retouched flakes, cores and Biface are recorded. They are discussed in the following schematic diagrams (Fig. 3.3.4; Fig. 3.3.5; Fig. 3.3.6 and Fig. 3.3.7).

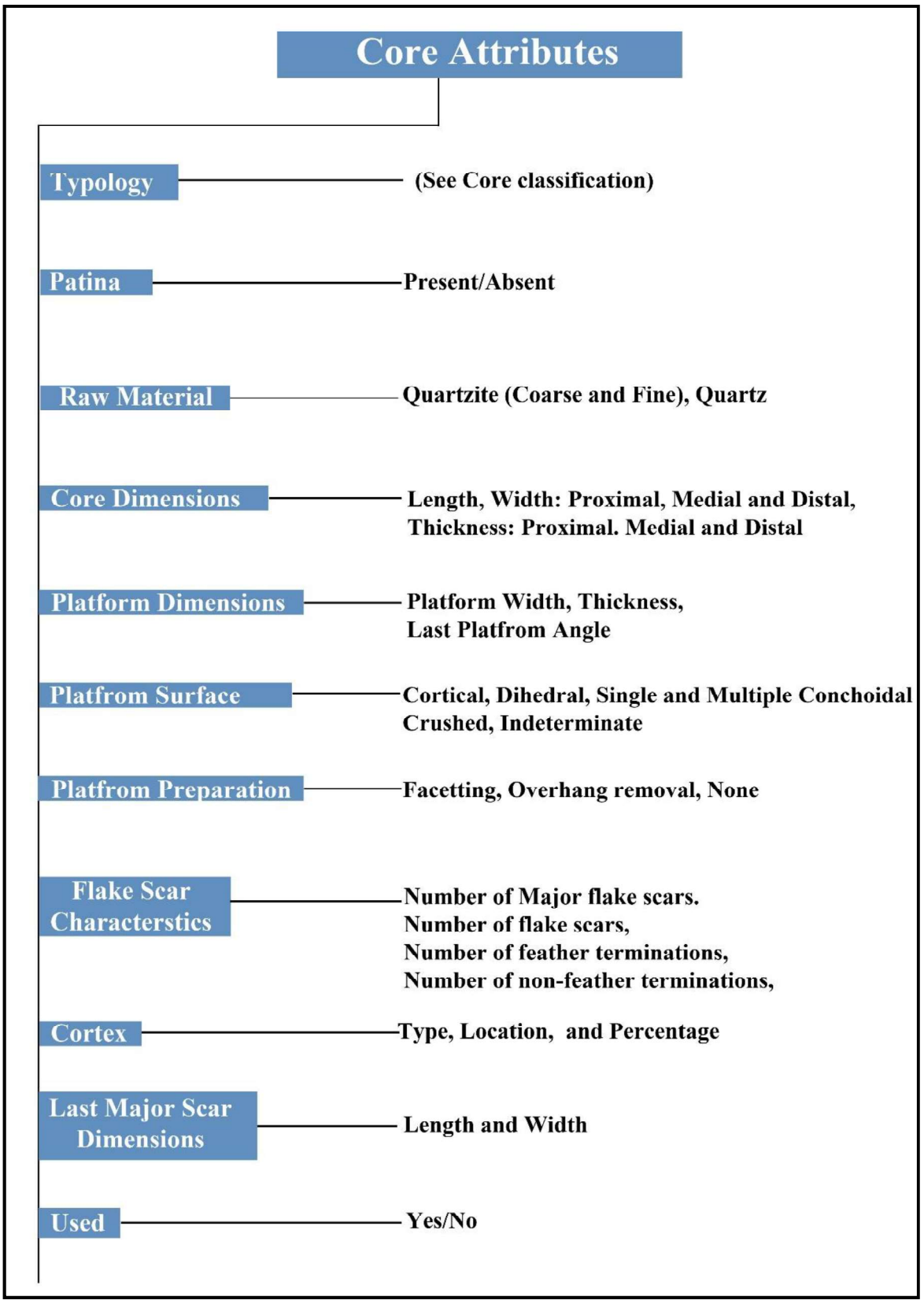

Figure. 3.3.4: Core attributes recorded in this study.

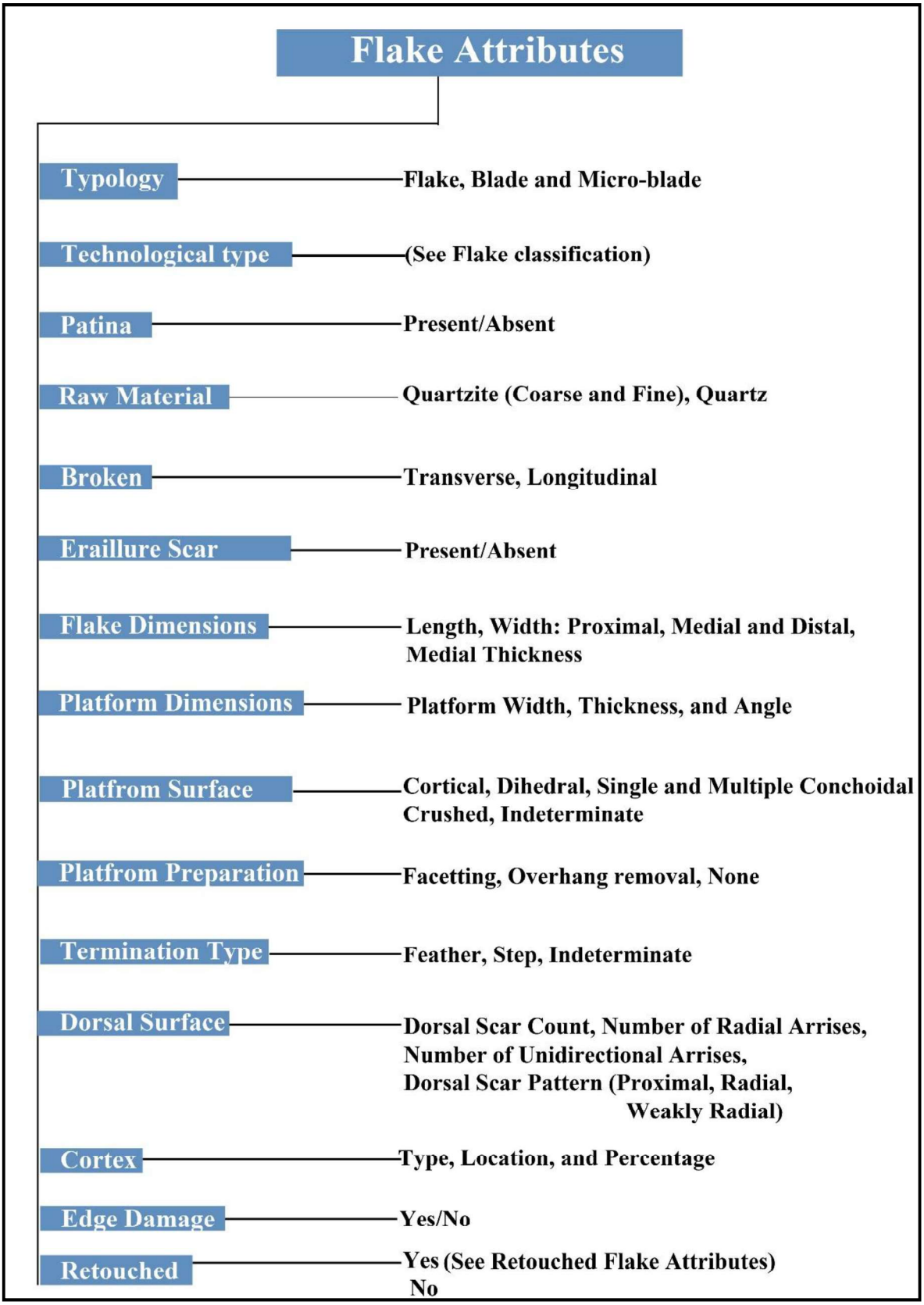

Figure. 3.3.5: Flake attributes recorded in this study.

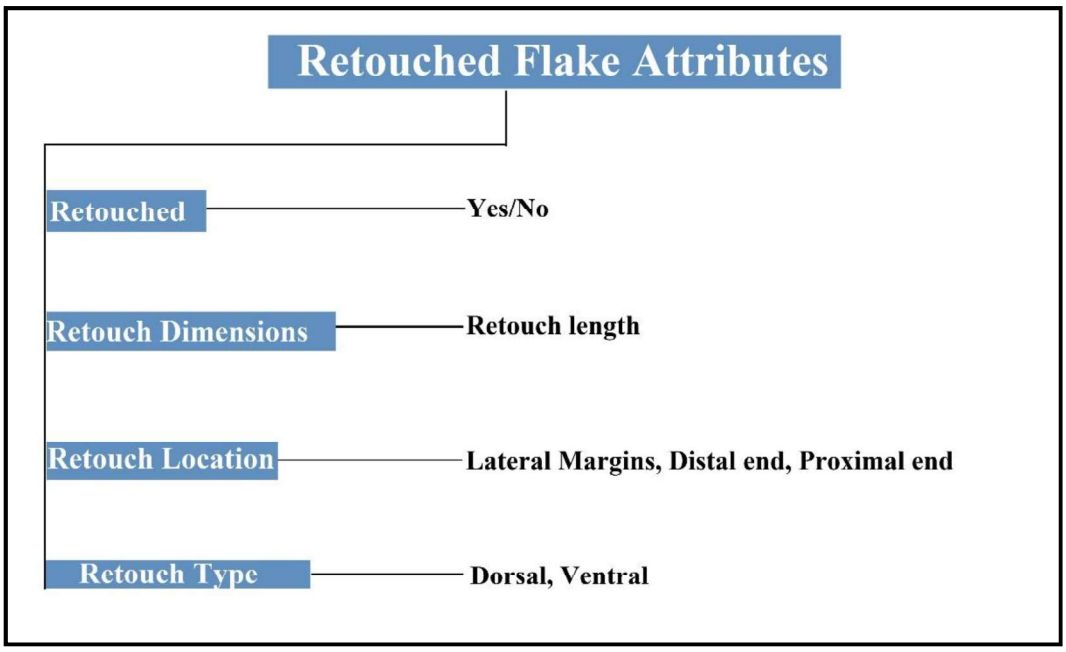

Figure. 3.3.6: Attributes recorded for retouched artefacts.

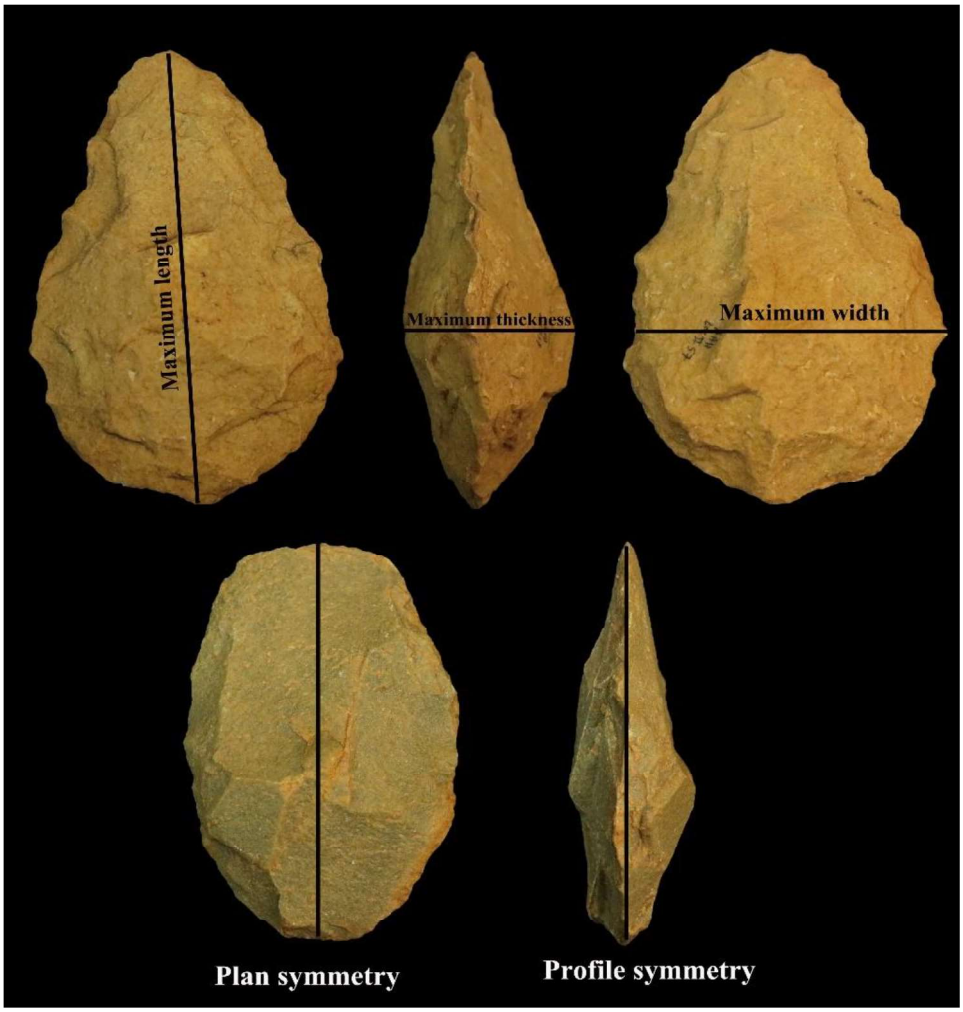

Figure. 3.3.7: Metrical attributes recorded for Bifaces.

A range of nominal, ordinal and scalar technological attributes have been recorded for each artefact based on the primary attributes that can be used to assess one or more aspects of the organization of technology. The attributes recorded and the aspects of the technological organization that can be inferred from them are presented in Table 3.3.1 to 3.3.2 and Fig. 3.3.8.

Table. 3.3.1: Attributes recorded on Cores indicating how they are recorded with relevant diagrams (modified after Blinkhorn, 2012).

Attribute	**Description**	**Reference**
Length	Length along the axis of the last percussion from the striking platform (mm)	Figure. 3.3.8
Proximal Width	Perpendicular to axial length at the proximal end of the core (mm)	
Medial Width	Perpendicular to axial length at mid-point of core (mm)	
Distal Width	Perpendicular to axial length at the distal end of the core (mm)	
Proximal Thickness	Perpendicular to Proximal Width (mm)	
Medial Thickness	Perpendicular to Medial Width (mm)	
Distal Thickness	Perpendicular to Distal Width (mm)	
Proximal shape	Axial Proximal Width/Axial Medial Width (1=parallel edges; >1=contracting edges; >1=expanding edges)	
Distal shape	Axial Medial Width/Axial Distal Width (1=parallel edges; >1=contracting edges; <1=expanding edges)	
Elongation	Axial Length/Axial Medial Width	
Flatness	Axial Medial Width/Medial Thickness	
Platform Preparation	Overhang removal (small flake scares – removed from the platform – at the proximal end on the dorsal face), Faceting (small flake scars on platform; removed from the proximal dorsal face)	
Platform Type	Cortical, Plain (no clear negative scar morphology), Single Conchoidal (single flake scar), Dihedral (sharp	

	angled intersection between two flake scars), Multiple Conchoidal (multiple flake scars), Punctiform (very thin surface), Crushed (fractured surface).	
Number of Core rotations	The number of times the flaking direction has changed	
Last platform angle	The angle between the last scar and the platform surface	
Number of major flake scars	Count of scars with length greater than 1/3 of core length	
Number of flake scars	Total flake scars	
Last termination type	Feather (tapered), Hinge (curved over), Step (broken), Outrepasse/Plunging (terminating on the surface opposite the flaking surface), Axial (split along the axis)	
Last major scar length	Axial length of the last scar >1/3 core length (mm)	Figure. 3.3.9
Last major scar width	Perpendicular to the Last Scar length at the mid-point of the scar (mm)	
Last major scar elongation	Last Scar Length/Last Scar Width	
Cortex %	Estimated at a 10% increment interval	

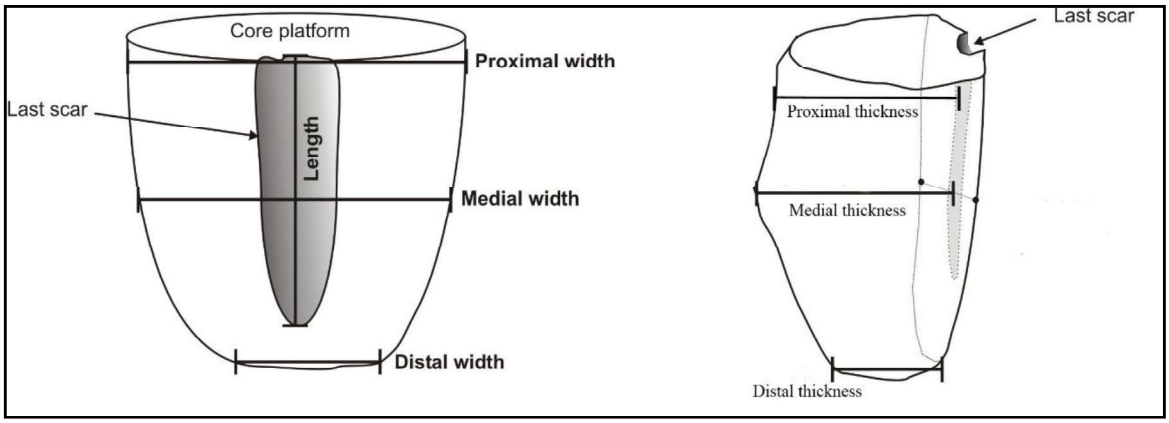

Figure. 3.3.8: Schematic sketch showing the recording of core dimensions (modified after Jones, 2007).

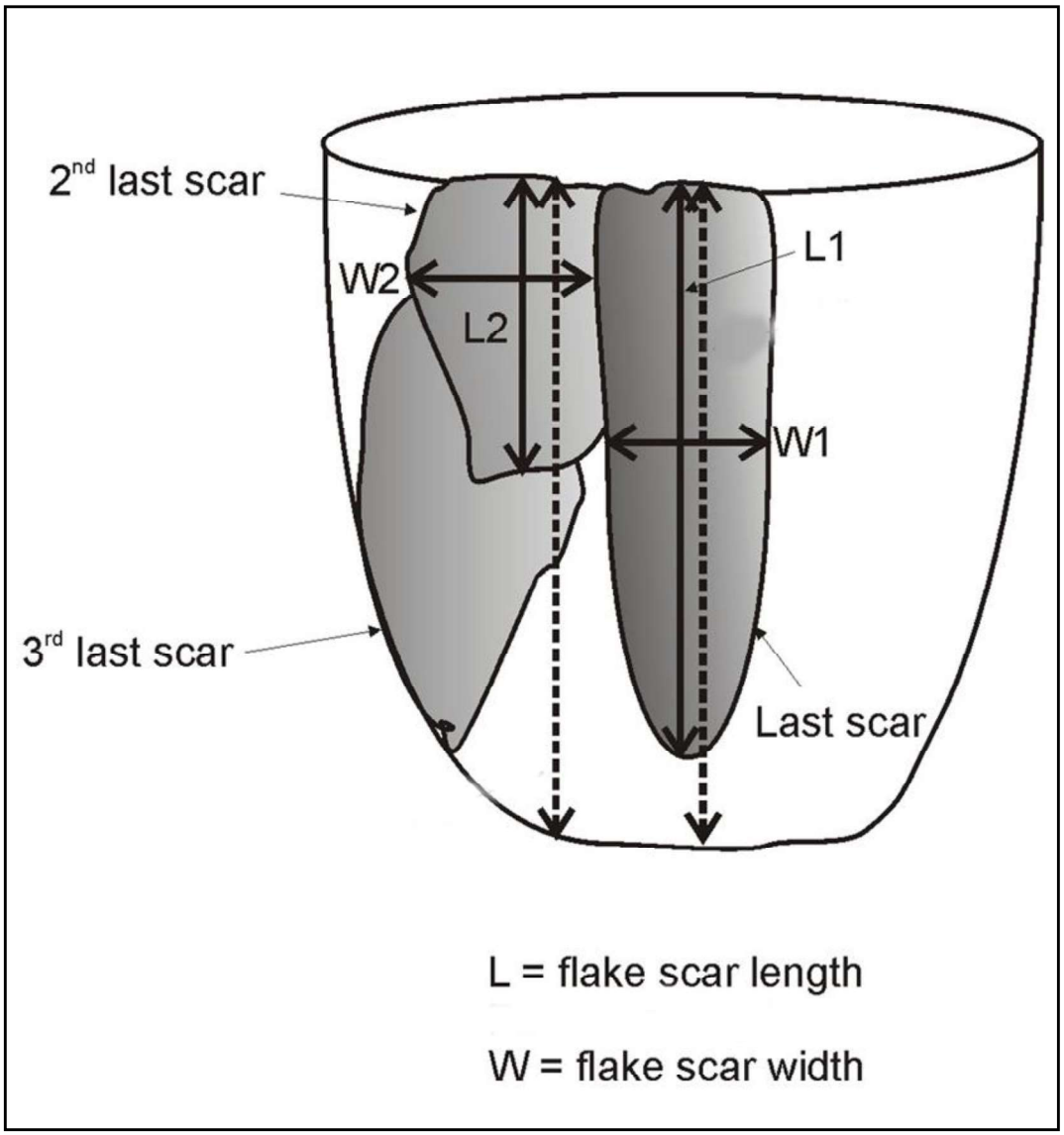

Figure. 3.3.9: Recording of last scar dimensions (modified after Jones, 2007).

Table. 3.3.2: Attributes recorded on Flakes indicating how they are recorded with relevant diagrams (modified after Blinkhorn, 2012).

Attribute	Description	Reference
Length	Length along the axis of percussions from the striking platform (mm)	Figure. 3.3.10
Proximal width	Perpendicular to axial length at proximal end of flake (mm)	
Medial width	Perpendicular to axial length at mid-point of flake (mm)	
Distal width	Perpendicular to axial length at distal end of flake (mm)	
Medial Thickness	Thickness at the mid-point of flake (mm)	
Platform width	Width of platform orientated by flaking axis (mm)	Figure. 3.3.11
Platform thickness	Perpendicular to platform width at the point of percussion (mm)	
Platform angle	the angle between the dorsal surface and the platform surface	
Platform type	Cortical, Plain (no clear negative flake scar morphology), Single Conchoidal (single flake scar), Dihedral (sharp angled intersection between two flake scars), Multiple Conchoidal (multiple flake scars), Punctiform (very thin surface), Crushed (fractured surface).	Figure. 3.3.12
Platform preparation	Overhang removal (small flake scares – removed from platform – at the proximal end of the dorsal face); Faceting (small flake scars – removed from the proximal dorsal face – on the platform)	Figure. 3.3.13
Termination type	Feather (tapered), Hinge (curved over), Step (broken), Outrepasse (terminating on the surface opposite to flaking surface), Axial (split along the axis)	Figure. 3.3.14
Dorsal scar count	Number of flake scars on the dorsal surface	

Dorsal scar pattern	Cortical (min 50% cortex cover and no clear flaking direction for removals on dorsal surface), Proximal (all scars originate from proximal), Distal (all scars originate from distal) Bidirectional (scars originate from proximal and distal), Opposed (scars originate from left and right), Perpendicular (scars originate from either a) proximal or distal and b) right and left), Weakly Radial (scars originate from three directions), Radial (scars originate from at least three directions and lack cortex)	Figure. 3.3.15
Number of unidirectional arrises	number of straight dorsal ridges that run 2/3 or more of the length of a flake that is unidirectionally flaked	Figure. 3.3.16
Number of radial arrises	number of dorsal ridges formed via radial flaking	
Retouch length	Straight length between start and end points of the longest retouched margin (mm)	
Retouch location	Lateral margins, distal or proximal ends	
Retouch type	on ventral or dorsal surface	
Elongation	Axial Length/Axial Medial Width	
Flatness	Axial Medial Width/Medial Thickness	
Proximal shape	Axial Proximal Width/Axial Medial Width (1=parallel edges; >1=contracting edges; <1=expanding edges)	
Distal shape	Axial Medial Width/Axial Distal Width (1=parallel edges; >1=contracting edges; <1=expanding edges)	

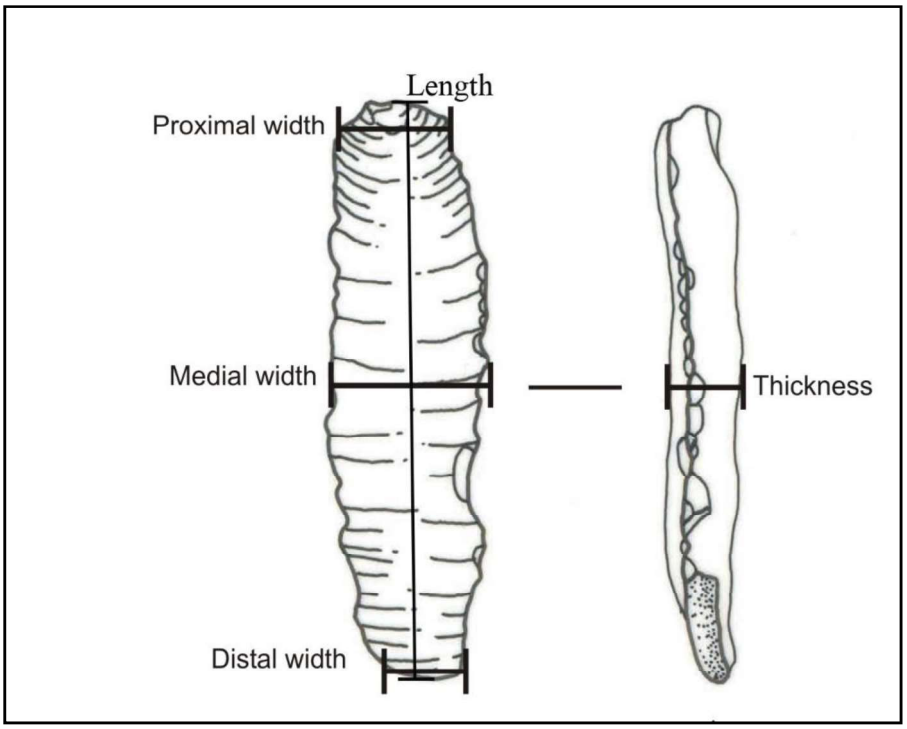

Figure. 3.3.10: Recording of Flake dimensions (modified after Jones, 2007).

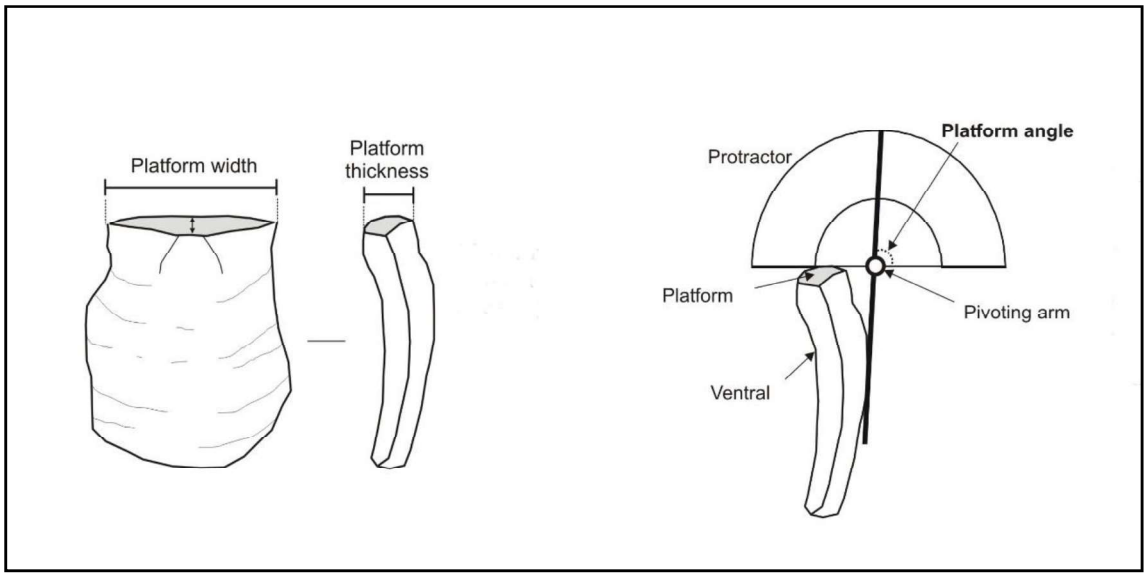

Figure. 3.3.11: Recording of flake platform dimensions (modified after Jones, 2007).

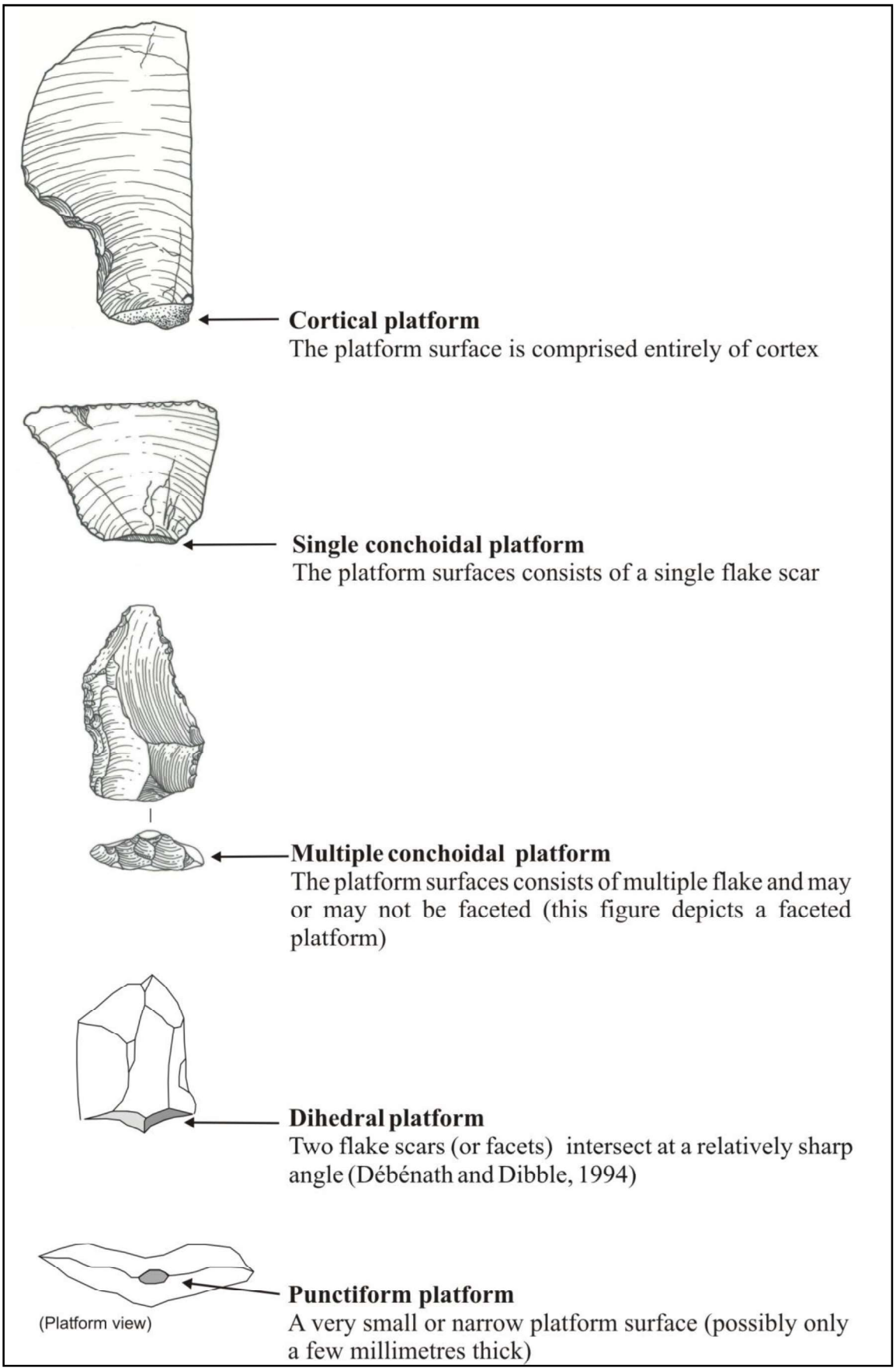

Figure. 3.3.12: Flake platform types recorded (Source: Jones, 2007).

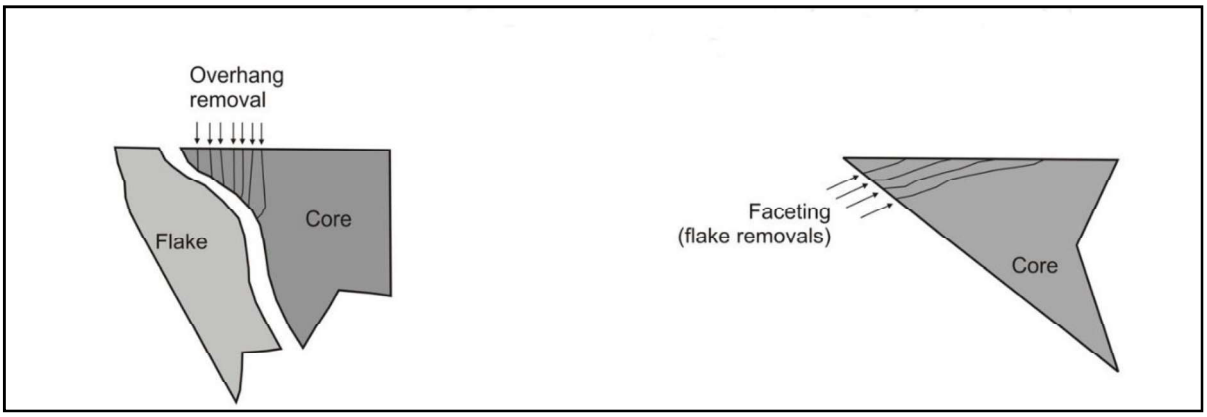

Figure. 3.3.13: Schematic sketch showing platform preparations (modified after Jones, 2007).

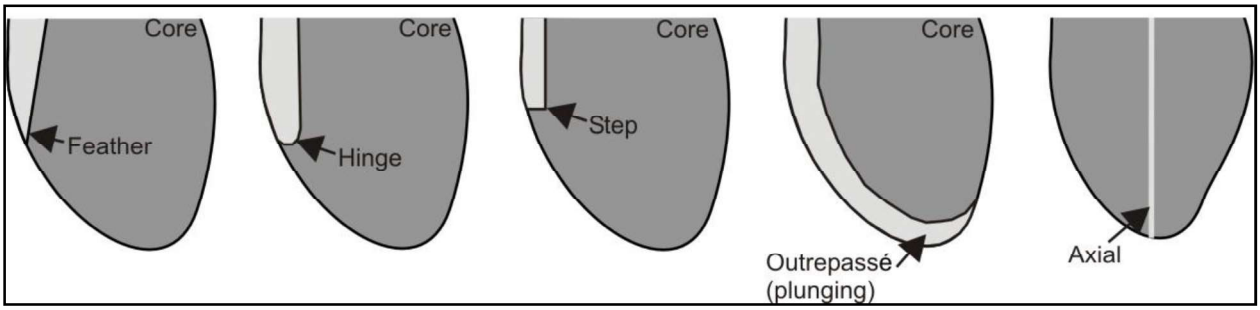

Figure. 3.3.14: Flake terminations recorded in this study (Source: Jones, 2007).

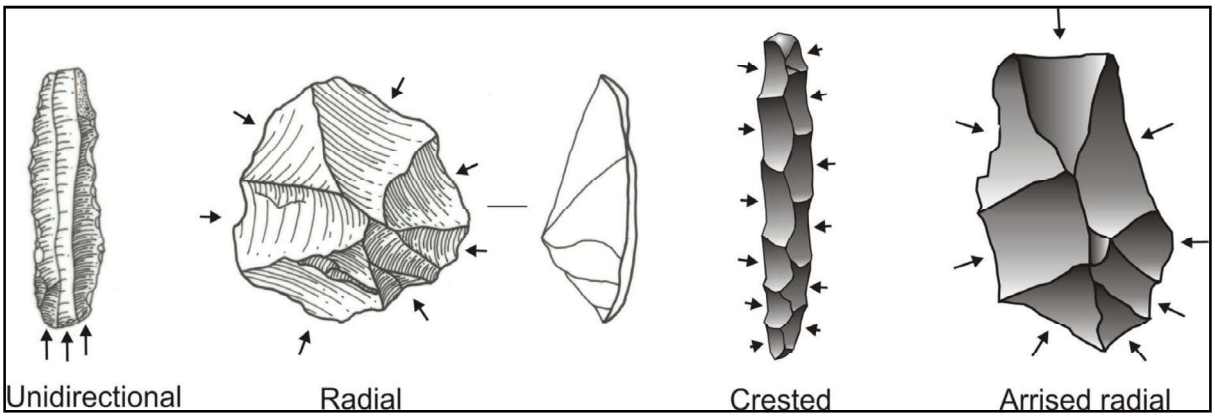

Figure. 3.3.15: Dorsal scar patterns recorded in this study (Source: Jones, 2007).

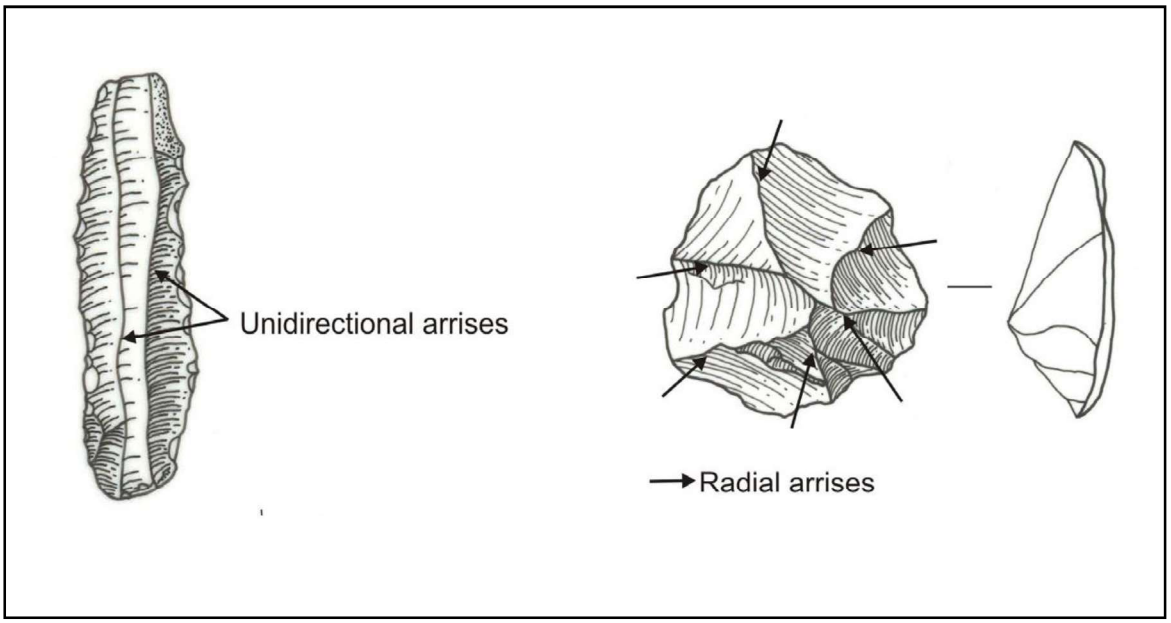

Figure. 3.3.16: Recording of type of arises on flakes dorsal surface (modified after Jones, 2007).

The discussion of lithic assemblages from the sites discussed in Chapters 4 and 5 includes a typological description of artefacts and a univariate description of artefact variability encompassing the entire assemblage. Preliminary testing has identified that the metric lithic attribute data are not normally distributed, and as a result, non-parametric tests have been used. Comparisons between more than two categories of numerical and ordinal data have been conducted using Kruskall-Wallis tests. Pair-wise comparisons of numerical and ordinal data, following Kruskall-Wallis tests, have been conducted using Mann-Whitney U-tests. Multi-variate analyses (Principal Component Analysis - PCA) are used around numerical and ordinal lithic attributes as well as artefact assemblages separated by time. For PCA analysis, the data sets were scaled and normalized using Box-Cox transformations before conducting the analysis. PCA analysis was done in the correlation matrix. All statistical analysis were done using the software PAST 4.11 (Hammer & Harper, 2005).